

QUANTIFYING THE EFFECT OF RANDOM SEAFLOOR ROUGHNESS ON HIGH-FREQUENCY SYNTHETIC APERTURE SONAR IMAGE STATISTICS

AP Lyons University of New Hampshire, Center for Coastal and Ocean Mapping, Durham,
New Hampshire, USA
DR Olson The Pennsylvania State University, Applied Research Laboratory, State College,
Pennsylvania, USA
RE Hansen Norwegian Defence Research Establishment (FFI), Kjeller, Norway

1 INTRODUCTION

Synthetic aperture sonar (SAS) is rapidly becoming a standard tool for seafloor imaging and target detection. An understanding of the physical processes affecting the acoustic scattering statistics of SAS images is a vital step toward fully utilizing the data produced by these systems for remote sensing or target detection applications. In regions with homogeneous geo-acoustic properties, the local texture seen in images from side-looking systems such as sidescan sonar or SAS are indicative of local, small-scale, seafloor slope variations. An Example SAS image taken in 2013 off the coast of Elba Island, Italy, by the Norwegian Defence Research Establishment (FFI), using the 100 kHz HISAS¹ mounted on a HUGIN AUV² is shown in Fig. 1 and clearly shows increasing variation in intensity as the range from the sonar increases. These increasingly strong intensity fluctuations as a function of range are due to the larger variation in scattering strength versus angle that exists at lower mean grazing angles. These fluctuations in intensity will modulate the imaging speckle, strongly influencing the overall statistical characteristics of SAS images³.

The continuous variation in scattering strength produced by a random slope field can be treated as an intensity scaling on the image speckle that is produced by the coherent SAS imaging process. Speckle can be described as multiplicative noise⁴ so that the overall statistics at any position in a SAS image can be expressed as the product of speckle noise and the scaling due to the underlying seafloor scattering cross section:

$$Y(r, x) = a(r, x)Z(r, x). \quad (1)$$

In Eq. (1), $Z(r, x)$ represents the speckle field for each pixel location in an image and $a(r, x)$ represents a modulating process which captures the effect of the random roughness induced intensity variation, and r and x , respectively, represent the down-range and cross-range (or along-track) image dimensions. In (1), $Y(r, x)$ is the matched-filtered and beam-formed intensity, so that speckle following a Rayleigh-distributed envelope would produce an exponentially distributed $Z(r, x)$ ⁵. As previously noted, the scaling function $a(r, x)$ is the acoustic expression of scattering from areas larger than the system's spatial resolution and is a function of the seafloor slope field. This scaling function is, effectively, a modulation of the scattering cross section, $\sigma_s(\theta)$, caused by local grazing angle changes due to variations of seafloor slope. The cross section term can be calculated via empirical or approximate models of seafloor interface scattering, such as Lambert's law, perturbation theory or the small-slope approximation.

In the sections that follow, we present a perturbation-theory based model which has been developed to predict the effect of random, power-law, roughness on the overall SAS image statistics. Changes in image statistics caused by roughness are quantified in terms of the relative intensity variance, or scintillation index (SI). Factors influencing the SI include the slope variance, geo-acoustic properties of the seafloor such as the sound speed ratio, the probability density function describing the speckle and the signal-to-noise ratio. Example model-data comparisons will be shown for SAS images taken in 2010 off the coast of Tellaro, Italy, by the NATO Undersea Research Centre, La Spezia, Italy, (now the NATO Centre for Maritime Research and

Experimentation) using the 300 kHz MUSCLE SAS system⁶, and for data collected with the Norwegian Defence Research Establishment's 100 kHz HISAS system off the coast of northwest coast of Elba Island, Italy, in 2013. Comparisons between parameter estimates obtained from high-resolution SAS data collected in these experiments and historical ground truth will be used to illustrate the efficacy of the model and its possible use for estimating roughness parameters, such as root-mean-square slope or height.

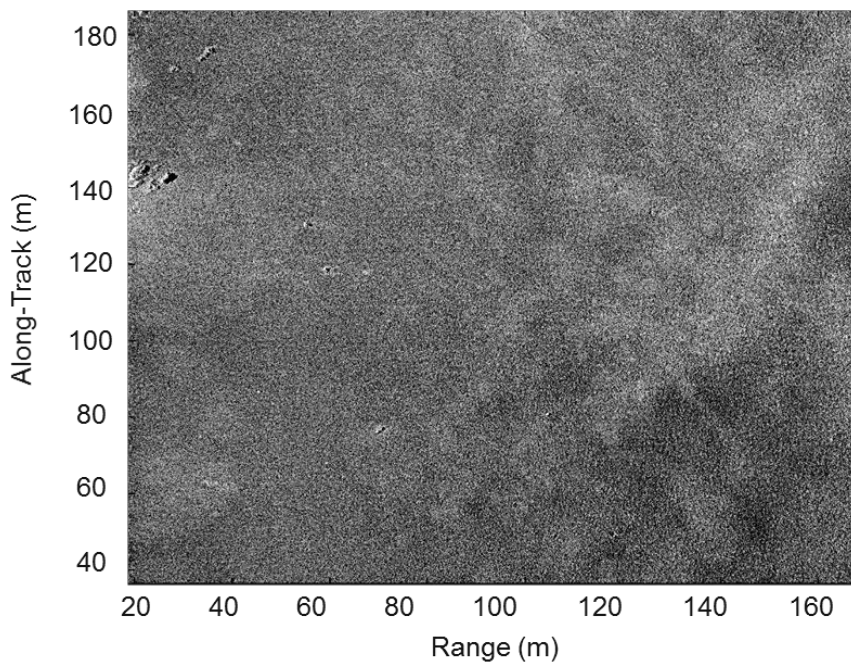


Figure 1: Synthetic aperture sonar image of a randomly rough sandy seafloor taken in 2013 off the northwest coast of Elba Island, Italy, using the Norwegian Defence Research Establishment's 100 kHz HISAS system.

2 MODELING THE EFFECT OF RANDOM ROUGHNESS ON IMAGE STATISTICS

For simplicity, we consider only the down-range dimension when relating the seafloor slope field to image statistics. The geometry for our problem is shown in Fig. 2, defining the true incident grazing angle interrogated by the sonar system, θ , the mean grazing angle, θ_0 , and the local slope angle, ϕ . The scattering strength will vary about its mean value as a function of range based on the relative (or local) grazing angle at a given range. The concept of larger-scale slopes modulating the scattering from smaller-scale roughness is similar conceptually to the composite roughness theory for seafloor backscatter⁷. Additive noise, σ_n , will also exist for any realistic sonar system. The scaling function, $a(r)$, which modulates the speckle intensity is therefore simply the scattering cross section evaluated at the true grazing angle with respect to the seafloor, $\theta = \phi - \theta_0$, at range, r , plus a noise term (assumed constant with range) expressed as a scattering cross section:

$$a(r) = \sigma_s(\phi - \theta_0) + \sigma_n. \quad (2)$$

The noise term is parameterized by θ_n defined by $\sigma_s(\theta_n) = \sigma_n$, the angle at which the noise term and seafloor scattering cross section are equal.

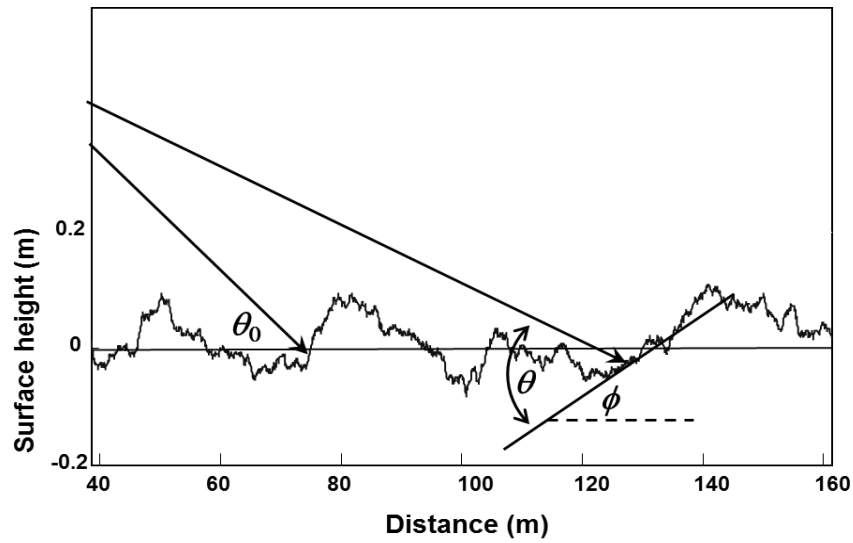


Figure 2: Geometry for the intensity-scaling problem. The rugged curve denotes the seafloor height field and the flat horizontal line the mean seafloor height (assumed to be zero). The true grazing angle, θ , of the incident acoustic field, the mean grazing angle, θ_0 , and the local slope angle, ϕ , are also denoted.

We quantify the changes in image statistics versus range caused by random roughness in terms of the normalized intensity variance, or scintillation index (SI). Note that higher values of SI are indicative of heavier-tailed scattered amplitude distributions and a value of 1 signifies a Rayleigh distribution. The scintillation index,

$$SI(r) = \frac{m_2 - m_1^2}{m_1^2} \quad , \quad (3)$$

representative of the image statistics at a given range, can be easily approximated in our case via knowledge of the intensity moments, m_1 and m_2 , of $Y(r)$. To facilitate analysis, local slope is treated as a continuous variable with range to yield the expected intensity moments,

$$m_n = E[Y^n] = \iint_{\mathcal{R}} a^n Z^n f(\phi) f(Z) d\phi dZ \quad , \quad (4)$$

where $f(\phi)$ is the slope distribution, assumed to be Gaussian with variance σ_g^2 :

$$f(\phi) = \frac{1}{\sqrt{2\pi}\sigma_g} \exp\left(-\phi^2/2\sigma_g^2\right) \quad . \quad (5)$$

The underlying speckle statistics are assumed to follow a K -distribution

$$f(Z) = \frac{4}{\sqrt{\lambda}\Gamma(\alpha)} \left(\frac{Z}{\sqrt{\lambda}}\right)^\alpha K_{\alpha-1}\left(\frac{2Z}{\sqrt{\lambda}}\right) \quad , \quad (6)$$

with shape parameter α and mean power λ (which we normalize to 1 in our analysis). In (6), $K_\nu(z)$ is the Basset function (i.e., a modified Bessel function of the third kind) and Γ is the gamma function.

This framework for modeling intensity statistics is similar in spirit to the procedure outlined in Hellequin, *et al.*⁸ who looked at the effects of random seafloor slope on the angular response of multibeam sonar backscatter statistics. We differ from that study, however, in that we perform a numerical integration of Eq. (3) and use perturbation theory⁹ instead of making an assumption that scattering strength versus grazing angle follows the empirical Lambert's law¹⁰. The effects of using the more realistic scattering theory will be examined in the next section.

From the previous equations, it is seen that if $a(r)$ is not constant then the image-level statistics will have a scintillation index greater than that expected for the underlying speckle statistics, i.e., have a heavier tailed distribution. The scintillation index also asymptotically approaches that of the underlying speckle (which itself may be very non-Rayleigh for small values of the K -distribution shape parameter) as the intensity scaling approaches a constant value (i.e., no slope-induced variability in the scattered power). At low grazing angles, the noise floor reduces the SI compared to the noise-free case. It should also be noted that when comparing these results to real data, system calibration is not necessary because any system dependent parameters such as vertical beam pattern would appear in both the numerator and denominator of Eq. (3) for a given range.

3 APPLICATION TO REAL SAS IMAGES

Having established the theoretical framework within which to interpret the effects of roughness-induced intensity scaling of the underlying speckle on the statistics of SAS images, we next investigate the applicability of these results by comparison to real data. Both the 100 kHz HISAS data taken off of Elba Island, Italy, in 2013 and the MUSCLE SAS data collected off of Tellaro, Italy, in 2010 will be compared to scintillation index predictions based on the scaled-speckle model. The MUSCLE SAS transmitted 60 kHz bandwidth signals at a center frequency of 300 kHz and the HISAS system transmitted 30 kHz bandwidth signals at a center frequency of 100 kHz. Images formed from the collected MUSCLE data had a resolution of approximately 1.5 cm in range x 2.5 cm along-track (cross-range) and images formed with HISAS data had a resolution of approximately 3.5 cm x 3.5 cm. The data from both the sites analyzed as part of this study were obtained on uniform and homogeneous seafloor areas of fine sands with varying degrees of topographic roughness, with the Elba experiment conducted in approximately 42 m water depth and the Tellaro experiment in 17 m water depth.

Fig. 3 shows experimental estimates of scintillation index versus range for the same HISAS data set that was used to form the example image shown in Fig 1. The experimental SI estimates have had outliers removed and have been smoothed with a 21-point averaging window. The scintillation index is seen to increase dramatically as a function of range (i.e., increase as the mean grazing angle decreases from approximately 26° at 40 m range to approximately 8° at 150 m range). It should be noted that it is not the underlying speckle statistics that are causing the overall increase in the scintillation index versus range, but the increasing slope of the scattering cross section versus grazing angle at further ranges (or smaller grazing angles). The scaled-speckle model developed in the previous section was used to predict the scintillation index using the rms seafloor slope as a free parameter and was fit to the experimental estimates of SI using known system geometries. Geo-acoustic input parameters for the perturbation theory-based model were found in Lyons *et al.*¹¹ for the same general vicinity as the Elba Island HISAS data collection site. A K -distribution shape parameter value of 3.0 was used in the model. This value was obtained using a method-of-moments estimator on data taken closest to the sonar in the image (i.e., with the largest mean grazing angles) where scattering strength is close to constant as a function of angle so that SI is driven solely by the speckle statistics. θ_n was set to 2° , but had little effect as this angle was quite far from the lowest angles in the image. An rms slope value of 5.2° was found to provide the best fit to the experimental data displayed in Fig. 3.

To illustrate the effect of the choice of scattering model, scintillation index was also calculated with the empirical Lambertian scattering model. The model results displayed in Fig. 3 show that SI increases much more quickly as range increases (as grazing angle decreases) for predictions

based on perturbation theory than for the Lambertian model. The intensity variability seen in an image at a specific range is directly related to the shape of the scattering strength curve, i.e., the rate of change of scattering strength as a function of angle. The approximately $\sin^4\theta$ dependence of scattering strength versus grazing angle at low angles for perturbation theory yields a larger SI for smaller grazing angles than the Lambertian case (with the same rms slope) while the relatively constant scattering strength versus angle near the critical angle of 27° yields a flatter curve of lower SI equal to that of the underlying speckle.

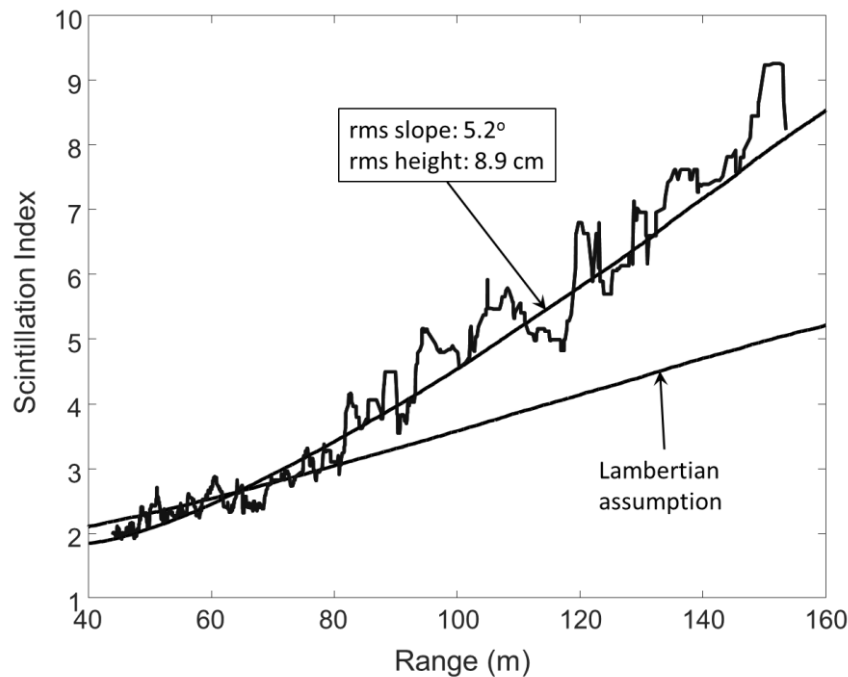


Figure 3: Scintillation index estimated from the HISAS data collected at Elba Island (rugged line) compared with a prediction made using the perturbation theory model for the scattering cross section in the scaled-speckle model. The Prediction made using the Lambertian model with the same rms slope as for perturbation theory model is also plotted.

Other statistical properties of the seafloor roughness can be obtained if a model of seafloor roughness is assumed. If a seafloor exhibits power-law roughness spectra, $W(k) = \beta k^{-\gamma}$, as has been frequently found⁹, rms height can be related to rms slope as outlined in Jackson *et al.*⁷. The rms seafloor height for the Elba data set, assuming power-law roughness, was found to be to 8.9 cm. For self-affine surfaces, such as those described by a power law, surface measures such as rms roughness, σ_h , will depend on largest observation length, l , and obey a scaling relationships of the form¹²

$$\sigma_h(l) = \sigma_h(l_0) \left(l/l_0 \right)^{(\gamma-2)/2} \quad (7)$$

Jackson and Richardson⁹ presented stereo-photogrammetry-based measurements of rms roughness of 0.2 to 1.0 cm for fine sands measured over scales on the order 100 cm. Using Eq. (7) with a spectral exponent of 3, these historical value of σ_h would yield rms roughness values over the much larger 150 m scale of the Elba SAS measurements of 3-12 cm, values which bracket the 8.9 cm rms roughness predicted by the scaled-speckle model.

A second data set used to explore the effects of random roughness on SAS image statistics consisted of data taken in 2010 off the coast of Tellaro, Italy, by the NATO Undersea Research Centre, La Spezia, Italy, (now the NATO Centre for Maritime Research and Experimentation) using a 300 kHz SAS mounted on the MUSCLE AUV. Example images are shown in Fig. 4. The top image in Fig. 4 clearly displays a larger variation in intensity than the bottom image which is caused in this case by larger undulations in seafloor slope. Fig. 5 shows estimates of scintillation index versus range estimated with the same the two MUSCLE data sets that were used to form the images shown in Fig. 4. As for the Elba Island HISAS data, the scintillation index is seen to increase as a function of range away from the sonar (i.e., SI increases as the mean grazing angle decreases from approximately 23° at 40 m range to approximately 7° at 150 m range). The large fluctuations in the scintillation index for the rough seafloor case (top curve) are due to shadowing from large seafloor structures visible in the top part of the image from approximately 90 m range, onward.

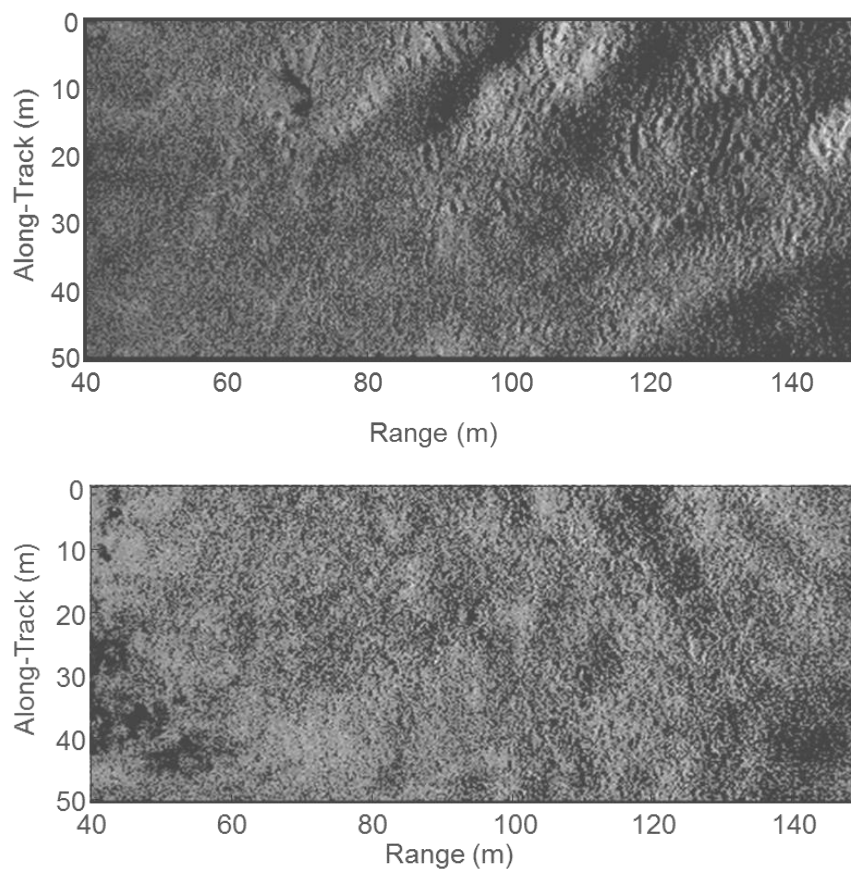


Figure 4: Synthetic aperture images of randomly rough silty-sand seafloors taken in 2010 off the coast of Tellaro, Italy, by the NATO Undersea Research Centre (now the NATO Centre for Maritime Research and Experimentation) with the 300 kHz MUSCLE SAS.

Geo-acoustic parameter inputs to the scattering model used for SI predictions for the Tellaro MUSCLE SAS data are from Pouliquen and Lyons¹³ which were obtained in the same water depth as and close to the location off of Tellaro, Italy, as the images shown in Fig. 1. A shape parameter of 2.75 was used in modeling SI, estimated in the same fashion as for the HISAS data discussed previously. Results shown on Fig. 5 are model predictions for rms slopes of 3.6° and 7.1° for the relatively smooth and relatively rough seafloor areas respectively. The model matches the shape of the data well and shows the sensitivity of the results to the rms slope. The rms seafloor height, assuming power-law roughness, were found to be to 2.9 cm and 5.8 cm for the smooth and rough

cases respectively. Data collected and presented in Pouliquen and Lyons¹³ from the same experimental area off of Tellaro used a stereo-photogrammetry system to measure rms roughness of 0.87 cm over a length scale of approximately 30cm. Using Eq. (7), this value of θ_h would yield an rms roughness over the much larger 50 m scale of the Tellaro SAS measurements of 6.4 cm very close to those predicted by the scaled-speckle model for the image of the “rough” area. A noise parameter, θ_n , of 5 was used for the MUSCLE system. As this value was close to the grazing angles interrogated at the furthest ranges in the images, the effects are more apparent as a more pronounced downward bending (i.e., reduction) of the SI when compared to the HISAS example.

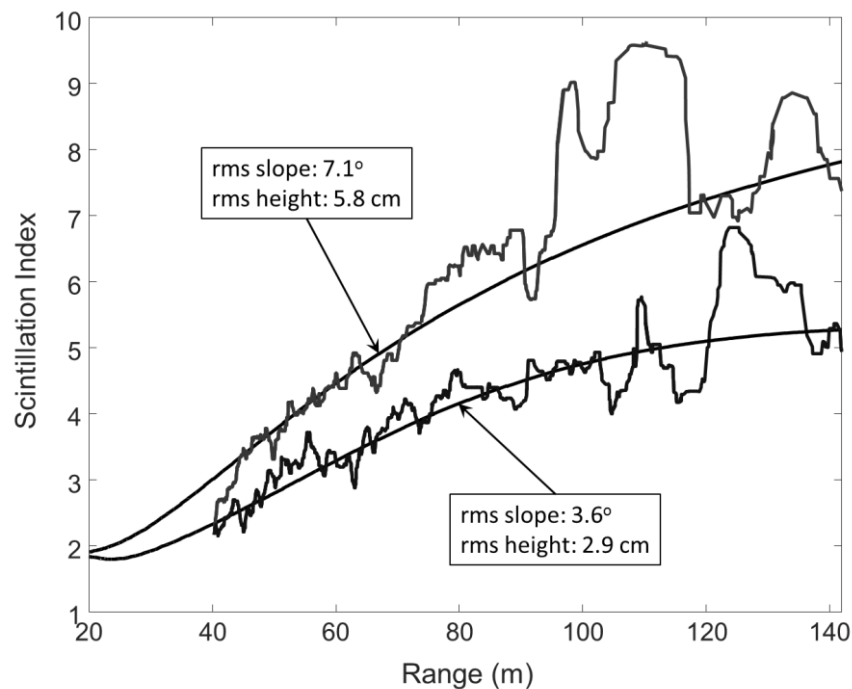


Figure 5: Scintillation index as a function of range for SAS images obtained from the Tellaro MUSCLE SAS field experiment (rugged line) and predictions from the scaled-speckle model. The experiment-derived curves used the same data that was used to form the images in Figure 4.

4 CONCLUSIONS

In this paper, we have presented a model to predict the impact of intensity scaling caused by random seafloor roughness on SAS image speckle statistics. This was accomplished by treating the continuous variation in scattering strength produced by roughness-induced changes in seafloor slope as a scaling of the SAS image speckle. The changes in image statistics were quantified in terms of the scintillation index. For the three experimental sites examined, roughness caused a dramatic effect on statistics of the images, with increasingly larger scintillation index (i.e., heavier-tailed distributions) as range away from the sonar increased. Scintillation index estimates from SAS data showed very good agreement with model predictions and were shown to be very sensitive to rms slope. This sensitivity could allow seafloor roughness parameters to be easily inverted from SAS image data as in Chen *et al.*¹⁴.

5 ACKNOWLEDGMENTS

The authors gratefully acknowledge Warren Fox, Hans Groen and others at the Centre for Maritime Research and Experimentation (CMRE), La Spezia, Italy, for allowing data from the AMiCa'10 sea trial to be used for this study. The authors also thank the CMRE for organizing the MANEX'13 trials onboard NRV Alliance and the Norwegian Defence Research Establishment for gathering the HISAS data with a HUGIN AUV during the trials. [For the work presented here, APL was supported under ONR Grants N00014-10-1-0051, N00014-10-1-0047 and N00014-10-1-0151 and DRO was supported under ONR Grant N00014-16-1-2335]

6 REFERENCES

1. T.G. Fossum, P.E. Hagen, B. Langli and R.E. Hansen, "HISAS 1030: High resolution synthetic aperture sonar with bathymetric capabilities," in Proc. Shallow Survey, Portsmouth, NH. (October 2008).
2. P. E. Hagen, N. J. Storkersen, and K. Vestgaard, "HUGIN—Use of UUV technology in marine applications," in Proc. MTS/IEEE OCEANS'99, 967–972. Seattle, WA (September 1999)
3. A.P. Lyons, D.A. Abraham and S.F. Johnson, "Modeling the effect of seafloor ripples on synthetic aperture sonar speckle statistics," IEEE J. Ocean. Eng., 35, 242-249. (2010).
4. F. Chaillan, C. Fraschini and P. Courmontagne, "Speckle noise reduction in SAS imagery," Signal Process., 87, 762–781. (2007).
5. A.P. Lyons and D.A. Abraham, "Statistical characterization of high-frequency shallow-water seafloor backscatter," J. Acous. Soc. Am., 106, 1307-1315 (1999).
6. A. Belletini and M. Pinto, "Design and experimental results of a 300-kHz synthetic aperture sonar optimized for shallow-water operations," IEEE J. Ocean. Eng., 34, 285-293. (2009).
7. D.R. Jackson, D.P. Winebrenner and A. Ishimaru, "Application of the composite roughness model to high-frequency bottom backscattering," J. Acous. Soc. Am., 79, 1410-1422. (1986).
8. L. Hellequin, J. Boucher and X. Lurton, "Processing of high frequency multibeam echosounder data for seafloor characterization," IEEE J. Ocean. Eng., 28, 78–89. (2003).
9. D.R. Jackson and M.D. Richardson, High-Frequency Seafloor Acoustics, (Springer, New York, 2007).
10. J. H. Lambert, "Photometria sive de mensura de gratibus luminis, colorum umbrae," (Eberhard Klett, Augsburg, 1760).
11. A.P. Lyons, S.F. Johnson, D.A. Abraham and E. Pouliquen, "High-frequency scattered envelope statistics of patchy seafloors," IEEE J. Ocean. Eng., 34, 451-458. (2009).
12. J.E. Summers, R.J. Soukup and R.F. Gragg, "Mathematical modelling and computer-aided manufacturing of rough surfaces for experimental study of seafloor scattering," IEEE J. Ocean. Eng., 32, 897-914. (2007).
13. E. Pouliquen and A.P. Lyons, "Backscattering from bioturbated sediments at very high frequency," IEEE J. Ocean. Eng., 27, 388-402. (2002).
14. C. Chen, A. Zare and J.T. Cobb, "Sand ripple characterization using an extended synthetic aperture sonar model and parallel sampling method," IEEE Trans. Geosci. Remote Sens., 53, 5547-5559. (2015).